Computers and Structures 295 (2024) 107294

Contents lists available at ScienceDirect

Computers and Structures

journal homepage: www.elsevier.com/locate/compstruc

Stability of the Bathe implicit time integration methods in the presence of physical damping

Chanju Lee [a], Klaus-Jürgen Bathe [b], Gunwoo Noh [a,*]

[a] Korea University, Seoul 02841, Republic of Korea
[b] Massachusetts Institute of Technology, Cambridge, MA 02139, USA

ARTICLE INFO

Keywords:
Direct time integration
Stability
Bathe method
Physical damping
Routh-Hurwitz criteria

ABSTRACT

Following the introduction of the standard Bathe implicit time integration scheme, there have been many research efforts in the development of time integration methods employing multi-step composite strategies. However, the stability analysis of these methods has been primarily conducted in the absence of physical damping, under the assumption that physical damping would render the analysis results more stable. This study demonstrates that physical damping can, in fact, impair the stability of a time integration. We consider the ρ_∞-Bathe and β_1/β_2- Bathe methods, and confirm that the use of the previously reported parameters is within the stable range in the presence of physical damping. For the β_1/β_2-Bathe method, a semi-analytic stability analysis provides an expanded range of applicable parameters. The results from the theoretical analysis are illustrated through simple numerical examples that could be used as benchmark problems to check the stability of a time integration method in the presence of physical damping.

1. Introduction

Direct time integration of finite element equations is extensively employed in analyzing structural response and wave propagations across various industries and scientific disciplines. While a linear analysis can be achieved using alternative approaches like the mode superposition method, nonlinear analysis typically necessitates a direct time integration [1–3]. Both explicit and implicit schemes are used for the integration. Explicit schemes, which are conditionally stable, require small time steps and are suitable for events such as crush simulations and wave propagations. In contrast, implicit schemes are generally unconditionally stable, allowing for larger time steps in structural dynamics and wave propagation simulations. Although implicit methods demand higher computational time per time step, their overall solution cost can be lower than that of explicit schemes [3]. Despite the availability of many implicit and explicit methods, the search for more efficient approaches has continued and any progress in effectiveness can deliver substantial benefits to both engineering and scientific studies [4–15].

A considerable amount of research has been dedicated to developing and optimizing time integration methods for structural dynamics and wave propagations. In recent years, the composite strategy with sub-steps has gained popularity, after the introduction of the standard Bathe method [14,15]. This implicit method has been well-received due to its ability to effectively suppress high-frequency inaccurate modes while maintaining accuracy in essential low-frequency modes. Researchers have since developed and investigated new implicit methods based on the composite strategy with sub-steps, see for example [16–37]. Furthermore, the multistep composite strategy has also been utilized in the development of explicit methods for structural dynamics and wave propagations [38–41].

During the development of time integration methods, the stability analysis was frequently conducted without considering the effects of physical damping, with the assumption that physical damping would enhance the stability of the method. However, as we shall see in the following sections, damping can, in fact, impair the stability of time integration methods, which can pose a significant problem for users.

In this study, we analyze the stability characteristics of the ρ_∞-Bathe [26–29] and β_1/β_2-Bathe methods [24,25] in the presence of physical damping. The paper is organized as follows. First, we introduce in Section 2 a semi-analytical stability analysis procedure using the Routh-Hurwitz criteria. Then, in Sections 3 and 4, we perform the stability analyses for the ρ_∞-Bathe and the β_1/β_2-Bathe methods, respectively. In Section 5 we illustrate our theoretical findings with two numerical

* Corresponding author.
E-mail address: gunwoonoh@korea.ac.kr (G. Noh).

https://doi.org/10.1016/j.compstruc.2024.107294
Received 24 October 2023; Accepted 19 January 2024
Available online 29 February 2024

examples. Finally, we summarize the main results.

2. Semi-analytical stability analysis

Considering linear analysis, the governing finite element equations in structural dynamics to be solved are

$$\mathbf{M}\ddot{\mathbf{U}} + \mathbf{C}\dot{\mathbf{U}} + \mathbf{K}\mathbf{U} = \mathbf{R} \tag{1}$$

with given initial conditions, where $\mathbf{M}$, $\mathbf{C}$ and $\mathbf{K}$ are the mass, damping and stiffness matrices and the vectors $\mathbf{U}$ and $\mathbf{R}$ list, respectively, the nodal displacements and externally applied nodal forces. An overdot denotes a time derivative.

The following decoupled modal equation can be considered to analyze the stability of time integration methods in linear analysis

$$\ddot{x} + 2\xi\omega\dot{x} + \omega^2 x = r \tag{2}$$

where ξ is the damping coefficient, ω is the natural frequency, r is the modal force, and x denotes the displacement in the modal space. With Eq. (2), a time integration method may be expressed as [3]

$$\begin{bmatrix} {}^{t+\Delta t}\ddot{x} \\ {}^{t+\Delta t}\dot{x} \\ {}^{t+\Delta t}x \end{bmatrix} = \mathbf{A}\begin{bmatrix} {}^{t}\ddot{x} \\ {}^{t}\dot{x} \\ {}^{t}x \end{bmatrix} + \mathbf{L_a}\,{}^{t+\gamma\Delta t}r + \mathbf{L_b}\,{}^{t+\Delta t}r \tag{3}$$

where $\mathbf{A}$, $\mathbf{L_a}$ and $\mathbf{L_b}$ are the integration approximation and load operators, respectively, and the left superscripts on x denote the discrete time point considered. The characteristic polynomial of the matrix $\mathbf{A}$ can be expressed as

$$p(\lambda) = \lambda^3 - A_1\lambda^2 + A_2\lambda - A_3 = 0 \tag{4}$$

where λ is an eigenvalue of $\mathbf{A}$, and A_i $(i = 1,\ 2,\ 3)$ are three principal invariants of the matrix:

$$A_1 = \mathrm{tr}(\mathbf{A}) = \lambda_1 + \lambda_2 + \lambda_3 \tag{5}$$

$$A_2 = \frac{1}{2}\left[(\mathrm{tr}(\mathbf{A}))^2 - \mathrm{tr}(\mathbf{A}^2)\right] = \lambda_1\lambda_2 + \lambda_2\lambda_3 + \lambda_3\lambda_1 \tag{6}$$

$$A_3 = \det(\mathbf{A}) = \lambda_1\lambda_2\lambda_3 \tag{7}$$

We utilize the Routh-Hurwitz criteria in the analysis of the stability characteristics [42], which for the above matrix, are written as follows

$$1 - A_1 + A_2 - A_3 \geq 0 \tag{8}$$

$$3 - A_1 - A_2 + 3A_3 \geq 0 \tag{9}$$

$$1 - A_2 + A_3(A_1 - A_3) \geq 0 \tag{10}$$

$$3 + A_1 - A_2 - 3A_3 \geq 0 \tag{11}$$

$$1 + A_1 + A_2 + A_3 \geq 0 \tag{12}$$

where the A_i $(i = 1,\ 2,\ 3)$ are functions of ω, ξ, Δt and the integration parameters.

When considering damping, an analytical evaluation of the inequalities (8–12) in order to obtain insight is difficult due to the complexity of the equations. Thus, to investigate the stability characteristics, we first identify the stability regions by evaluating the solvable inequalities, accounting for both, the damped and undamped cases. Then we perform a numerical verification to ensure that the defined regions in fact satisfy all the inequalities – this complete procedure is hence a semi-analytical stability analysis.

Note that for methods utilizing equilibrium at time $t + \Delta t$, like the Bathe methods, the matrix $\mathbf{A}$ can be reduced to a 2 by 2 matrix. Then, only three inequalities are considered in the Routh-Hurwitz criteria. On the contrary, for methods not strictly satisfying the equilibrium at $t + \Delta t$, such as the three-parameter method or the generalized-α method [7,8], $\mathbf{A}$ should be of size 3 by 3. To illustrate the general procedure, we will use inequalities (8–12) with Eq. (3) in the following sections.

3. Stability analysis of the ρ_∞-Bathe time integration scheme

We start with the analysis of the ρ_∞-Bathe scheme which is a very general procedure, containing as a special scheme also the Newmark method with the parameters mostly used [27].

3.1. The ρ_∞-Bathe time integration scheme

The governing finite element equations of structural dynamics to be solved are Eq. (1). If the time step size Δt is set and all solution variables are known up to time t, then the time integration scheme calculates the solution at time $t + \Delta t$.

The ρ_∞-Bathe method [26] involves determining the nodal displacements, velocities, and accelerations at time $t + \Delta t$ through a two-sub-step process in which the time step Δt is partitioned into two sub-steps of sizes $\gamma\Delta t$ and $(1-\gamma)\Delta t$. In the first sub-step of the ρ_∞-Bathe scheme, as in the standard Bathe method, we use the trapezoidal rule for the equilibrium at time $t + \gamma\Delta t$.

$$\mathbf{M}\,{}^{t+\gamma\Delta t}\ddot{\mathbf{U}} + \mathbf{C}\,{}^{t+\gamma\Delta t}\dot{\mathbf{U}} + \mathbf{K}\,{}^{t+\gamma\Delta t}\mathbf{U} = {}^{t+\gamma\Delta t}\mathbf{R} \tag{13}$$

$${}^{t+\gamma\Delta t}\mathbf{U} = {}^{t}\mathbf{U} + \frac{\gamma\Delta t}{2}\left({}^{t}\dot{\mathbf{U}} + {}^{t+\gamma\Delta t}\dot{\mathbf{U}}\right) \tag{14}$$

$${}^{t+\gamma\Delta t}\dot{\mathbf{U}} = {}^{t}\dot{\mathbf{U}} + \frac{\gamma\Delta t}{2}\left({}^{t}\ddot{\mathbf{U}} + {}^{t+\gamma\Delta t}\ddot{\mathbf{U}}\right) \tag{15}$$

and in the second sub-step, we use the following relations with the parameters $q_0,\ q_1,\ q_2,\ s_0,\ s_1,\ s_2$ for the equilibrium at time $t + \Delta t$,

$$\mathbf{M}\,{}^{t+\Delta t}\ddot{\mathbf{U}} + \mathbf{C}\,{}^{t+\Delta t}\dot{\mathbf{U}} + \mathbf{K}\,{}^{t+\Delta t}\mathbf{U} = {}^{t+\Delta t}\mathbf{R} \tag{16}$$

$${}^{t+\Delta t}\mathbf{U} = {}^{t}\mathbf{U} + \Delta t\left(q_0\,{}^{t}\dot{\mathbf{U}} + q_1\,{}^{t+\gamma\Delta t}\dot{\mathbf{U}} + q_2\,{}^{t+\Delta t}\dot{\mathbf{U}}\right) \tag{17}$$

$${}^{t+\Delta t}\dot{\mathbf{U}} = {}^{t}\dot{\mathbf{U}} + \Delta t\left(s_0\,{}^{t}\ddot{\mathbf{U}} + s_1\,{}^{t+\gamma\Delta t}\ddot{\mathbf{U}} + s_2\,{}^{t+\Delta t}\ddot{\mathbf{U}}\right) \tag{18}$$

where the parameters are

$$\begin{aligned} q_0 &= (\gamma-1)q_1 + \frac{1}{2},\quad q_2 = -\gamma q_1 + \frac{1}{2}, \\ s_0 &= (\gamma-1)s_1 + \frac{1}{2},\quad s_2 = -\gamma s_1 + \frac{1}{2},\quad s_1 = q_1 \end{aligned} \tag{19}$$

$$q_1 = \frac{\rho_\infty + 1}{2\gamma(\rho_\infty - 1) + 4} \tag{20}$$

The relation in Eq. (20) is used to directly prescribe the amount of numerical dissipation in the high-frequency range by specifying γ and ρ_∞.

3.2. Semi-analytical stability analysis of the ρ_∞-Bathe time integration scheme

We perform the analytical analysis in two cases: with and without damping. In the presence of ξ, only (8) can be solved analytically for the ρ_∞-Bathe method. Using the principal invariants of the ρ_∞-Bathe method, the inequality (8) can be expressed as

$$\begin{aligned} 1 - A_1 + A_2 - A_3 = -\frac{1}{2\chi}\Omega^2 &\left(\begin{array}{l} 4 + \Omega^2(\rho_\infty-1)^2\gamma^4/4 + (\rho_\infty-1)^2\Omega(\xi - \Omega/2)\gamma^3 \\ -(\rho_\infty-1)\left((-\rho_\infty/4 + 1/4)\Omega^2 + \xi(\rho_\infty - 3)\Omega - \rho_\infty + 1\right)\gamma^2 \\ -2(\rho_\infty-1)(\Omega\xi - 2)\gamma \end{array}\right) \\ &\geq 0 \end{aligned} \tag{21}$$

where

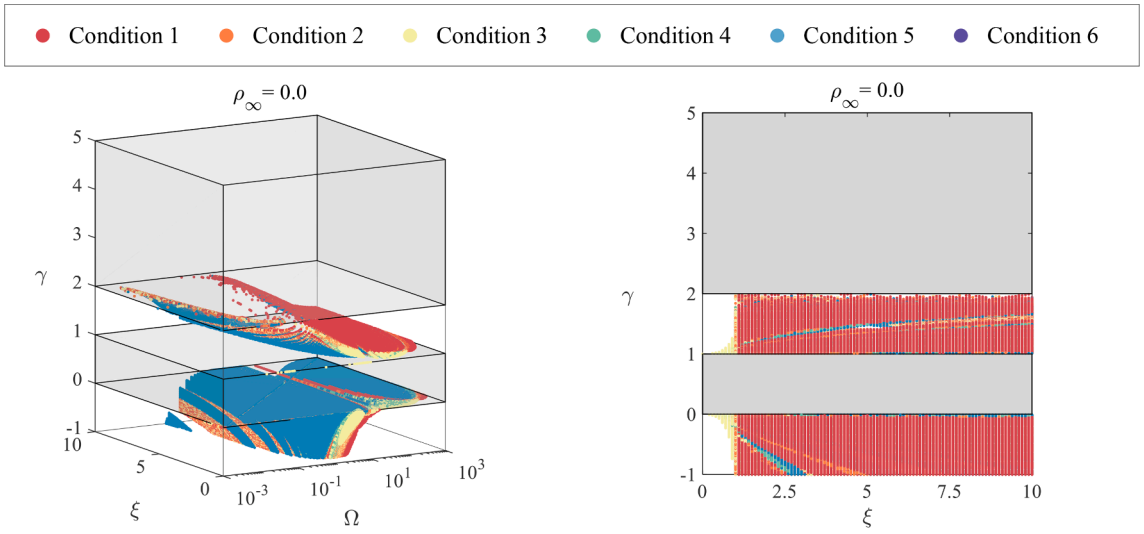

(a) Data points violating the conditions (b) Projection of Fig. 1(a) onto the ξ and γ plane

Fig. 1. Numerical test results of the ρ_∞-Bathe method when ρ_∞=0; Conditions (1–5) are associated with inequalities (8–12). Condition 6 is violated when yielding a complex number. The gray-shaded regions, $0 < \gamma < 1$ and $2 < \gamma$, denote the regions of stability from (23) for ρ_∞=0.

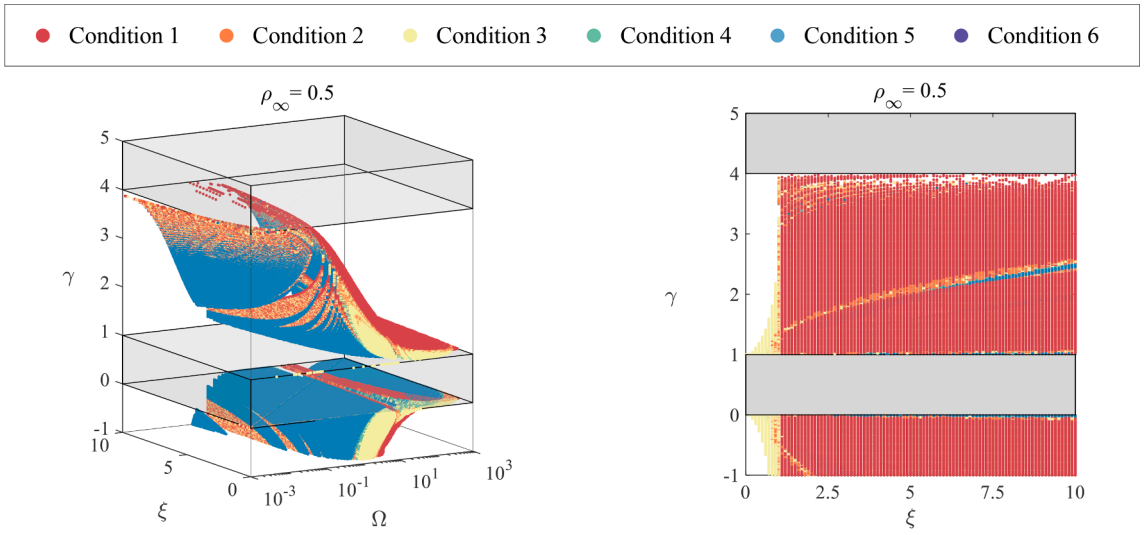

(a) Data points violating the conditions (b) Projection of Fig. 2(a) onto the ξ and γ planes

Fig. 2. Numerical test results of the ρ_∞-Bathe method when ρ_∞=0.5; Conditions (1–5) are associated with inequalities (8–12). Condition 6 is violated when yielding a complex number. The gray-shaded regions, $0 < \gamma < 1$ and $4 < \gamma$, denote the regions of stability from (23) for ρ_∞=0.5.

$$\chi = (\Omega^2\gamma^2/4 + \Omega\gamma\xi + 1)\left(\begin{array}{l}\left(\text{-}\Omega^2/2 + \xi(\rho_\infty - 1)\Omega\text{-}(\rho_\infty - 1)^2/2\right)\gamma^2 - 2+ \\ (\Omega^2\text{-}\xi(\rho_\infty\text{-}3)\Omega\text{-}2\rho_\infty + 2)\gamma\text{-}2\Omega\xi\text{-}\Omega^2/2\end{array}\right)$$

and Ω=$\omega\Delta t$ with ω the natural frequency. To satisfy (8), $1 - A_1 + A_2 - A_3$ should be positive for all $\Omega > 0$. The two solutions of Ω that satisfies $1 - A_1 + A_2 - A_3 = 0$ are

$$\Omega_{\xi\neq 0} = 0 \text{ and } \frac{2\left(-\xi \pm \sqrt{\xi^2 - 1}\right)(\gamma\rho_\infty - \gamma + 2)}{(\gamma - 1)(\rho_\infty - 1)\gamma} \tag{22}$$

With $\xi \geq 0$ and $-1 \leq \rho_\infty < 1$, the stable range of γ is determined by the conditions $\Omega_{\xi\neq 0} \leq 0$ or the condition $\Omega_{\xi\neq 0}$ tending to infinity, in order to satisfy inequality (8). Note that the values γ=0, 1 and $2/(1 - \rho_\infty)$ also need to be avoided to not have a zero denominator of constants in the method when implemented. Therefore, the applicable range of γ that satisfies the stability conditions is

$$\gamma \in (0, 1) \cup \left(\frac{2}{1 - \rho_\infty}, \infty\right) \text{ if } \rho_\infty \neq -1 \tag{23}$$

Setting ξ=0, a further analytical analysis to identify under what conditions the inequalities (8–10) are satisfied can be conducted. Again, we consider the values of Ω for the left-hand sides of the inequalities to be zero

$$\Omega_{(8),\xi=0} = 0 \text{ or } \frac{\pm 2i\,(\gamma\rho_\infty - \gamma + 2)}{(\gamma - 1)(\rho_\infty - 1)\gamma} \tag{24}$$

$$\Omega_{(9),\xi=0} = 0 \text{ or } \frac{\pm 2\,(\gamma\rho_\infty - \gamma + 2)}{(\gamma - 1)\,\gamma\sqrt{\rho_\infty^2 + 2\rho_\infty - 3}} \tag{25}$$

$$\Omega_{(10),\xi=0} = 0 \tag{26}$$

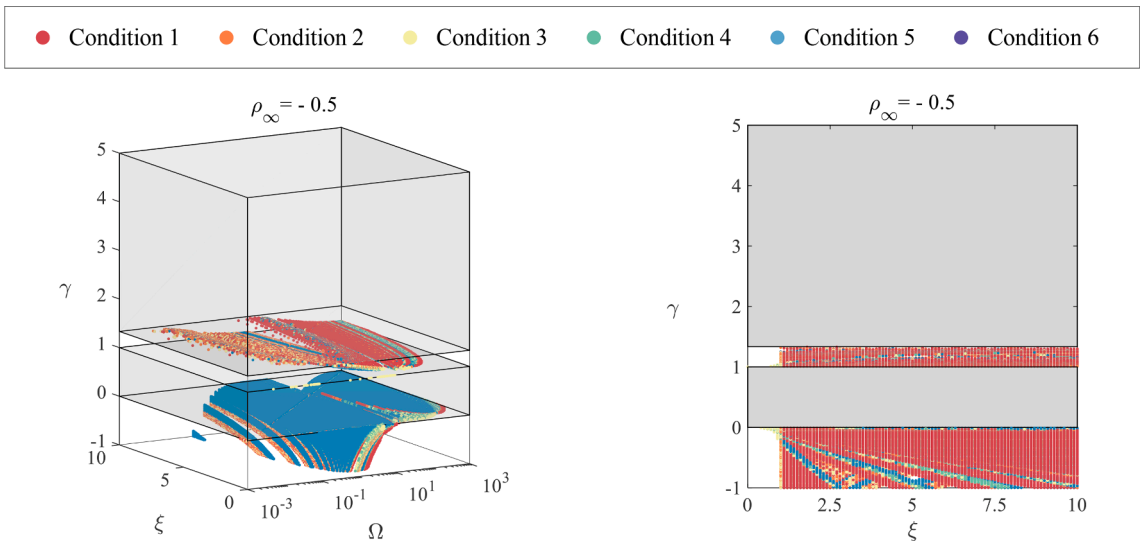

(a) Data points violating the conditions

(b) Projection of Fig. 3(a) onto the ξ and γ plane

Fig. 3. Numerical test results of the ρ_∞-Bathe method when ρ_∞=−0.5; Conditions (1–5) are associated with inequalities (8–12). Condition 6 is violated when yielding a complex number. The gray-shaded regions, $0 < \gamma < 1$ and $4/3 < \gamma$, denote the regions of stability from (23) for ρ_∞=-0.5.

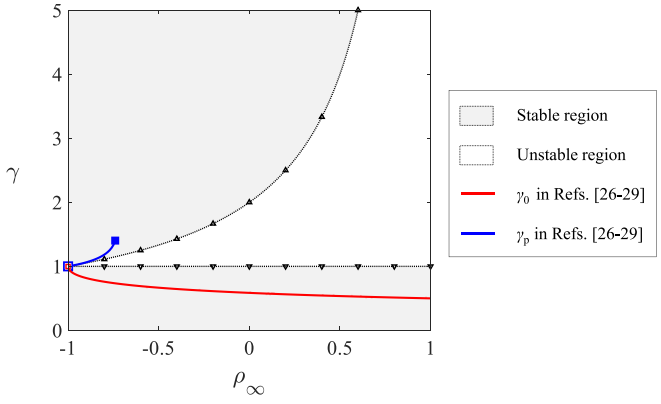

Fig. 4. The optimized splitting ratios γ_0 and γ_p as a function of ρ_∞ when damping is present; Both values γ_0 and γ_p are within the stable regions.

Then, as Ω is a positive real number and $-1 \leq \rho_\infty < 1$, it is clear that the inequalities (8–10) are satisfied for all γ and ρ_∞, when ξ=0. Therefore, from the analysis of the analytically solvable inequalities – the inequality (8) in the presence of physical damping and the inequalities (8–10) for the case of zero damping – we obtain the necessary condition for stability given in (23).

Note that when ρ_∞ = -1, the values of the inequalities (8–12) can be written

$$1 - A_1 + A_2 - A_3 = \frac{4\,\Omega^2}{\Omega^2 + 4\Omega\xi + 4} \tag{27}$$

$$3 - A_1 - A_2 + 3A_3 = \frac{4\,\Omega(\,\Omega + 4\xi)}{\Omega^2 + 4\Omega\xi + 4} \tag{28}$$

$$1 - A_2 + A_3(A_1 - A_3) = \frac{8\,\Omega\xi}{\Omega^2 + 4\Omega\xi + 4} \tag{29}$$

$$3 + A_1 - A_2 - 3A_3 = \frac{16\,\Omega\xi + 16}{\Omega^2 + 4\Omega\xi + 4} \tag{30}$$

$$1 + A_1 + A_2 + A_3 = \frac{16}{\Omega^2 + 4\Omega\xi + 4} \tag{31}$$

Thus, all the conditions are unconditionally satisfied and therefore when ρ_∞ = -1, the method is stable regardless of the value of γ.

Meanwhile, when $\rho_\infty = 1$, the inequalities (8–10) and (12) can be analytically solved, and the values of Ω for which the left-hand side of each inequality becomes zero are

$$\Omega_{(8),\xi\neq 0} = 0 \tag{32}$$

$$\Omega_{(9),\xi\neq 0} = 0 \text{ or } \frac{1 \pm \sqrt{16\gamma^2\xi^2 - 16\xi^2\gamma + 1}}{2\gamma\xi(\gamma - 1)} \tag{33}$$

$$\Omega_{(10),\xi\neq 0} = 0 \text{ or } \pm\frac{2}{\sqrt{\gamma^2 - \gamma}} \tag{34}$$

$$\Omega_{(12),\xi\neq 0} = \pm\frac{2\sqrt{\gamma(\gamma-1)\left(2\xi^2 + 2\sqrt{\xi^4 - \xi^2} - 1\right)}}{\gamma(\gamma-1)} \text{ or } \pm\frac{2\sqrt{-\gamma(\gamma-1)\left(-2\xi^2 + 2\sqrt{\xi^4 - \xi^2} + 1\right)}}{\gamma(\gamma-1)} \tag{35}$$

Therefore, when $\rho_\infty = 1$, the applicable stable range is $\gamma \in (0, 1)$ which is consistent with (23).

In Ref. [26], the stability of the technique was examined in the absence of damping; however, the presence of damping leads to unstable results when deviating from (23) (see also Section 5).

We therefore examine possible violations of the inequalities numerically. We consider various values of Ω, ξ and γ; the values of Ω vary in the ranges [0.001, 0.1], [0.1, 10], and [10, 1000], with spacings of 0.001, 0.1, and 10, respectively, ξ is varied over the range [0, 10] with a spacing of 0.1, and the splitting ratio γ is varied over the range [-1, 5] with a spacing of 0.01. Note that in a mode superposition solution, we have typically $0 \leq \xi < 1$, and ξ is generally small. In contrast, in a direct integration solution, stiffness proportional damping might result in a significantly larger value; consequently, we incorporate ξ values up to 10. Also, for an expedient numerical test, we could confine our numerical tests only to the range of necessary conditions for stability

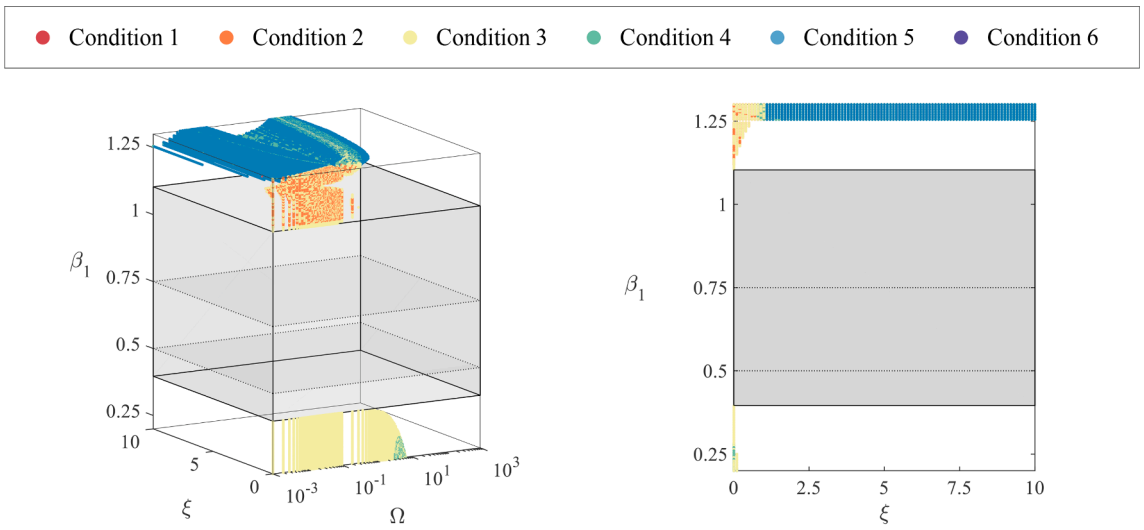

(a) Data points violating the conditions

(b) Projection of Fig. 5(a) onto the ξ and β_1 plane

Fig. 5. Numerical test results of the β_1/β_2-Bathe method when $\gamma = (\beta_2 - 1)/(2\beta_1 - 2 + \beta_2)$ and $\beta_2 = 1/(3 - 4\beta_1)$; Conditions (1–5) are associated with inequalities (8–12). Condition 6 is violated when yielding a complex number. The gray-shaded regions, $\left(\frac{3}{4} - \frac{\sqrt{2}}{4}\right) \le \beta_1 \le \left(\frac{3}{4} + \frac{\sqrt{2}}{4}\right)$, denote the region of stability from (50). $\beta_1 =$ 0.5 and 0.75 should be avoided to maintain the non-zero denominators.

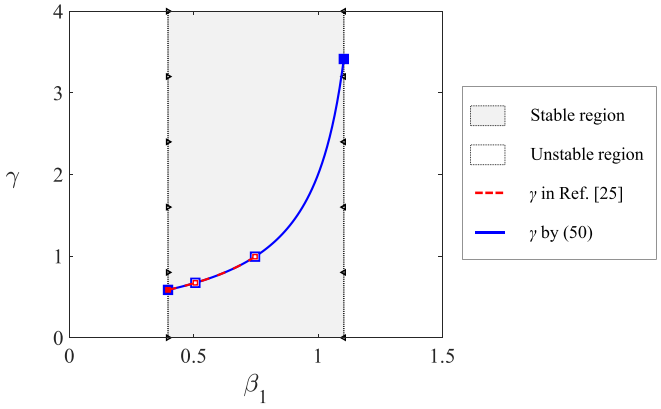

Fig. 6. The splitting ratio γ as a function of β_1 for the β_1/β_2-Bathe method with $\gamma = (\beta_2 - 1)/(2\beta_1 - 2 + \beta_2)$ and $\beta_2 = 1/(3 - 4\beta_1)$; The previously reported ranges of β_1 in Ref. [25] are within the stable region shown in (50).

already determined analytically.

We checked on a total of six conditions: in addition to those denoted as Conditions (1–5), corresponding to inequalities (8–12), we use a Condition 6, that the splitting ratio γ not be a complex number.

Fig. 1 illustrates the numerical test results for the ρ_∞-Bathe method with $\rho_\infty = 0$. Distinct colors denote data points that breach specific conditions. The defined ranges that adhere to the necessary conditions in (23) for $\rho_\infty = 0$ are $0 < \gamma < 1$ and $2 < \gamma$. These areas are represented by gray shading. Notably, there are no colored data points, indicating violations, within this shaded region. Conversely, values of γ outside the range shown in (23) fail to satisfy at least one inequality. Figs. 2 and 3 display results for $\rho_\infty = 0.5$ and $\rho_\infty =$ -0.5, respectively, reaffirming that data within the stable γ range derived from (23) comply with all conditions.

In Refs. [26–29], the following optimized splitting ratios γ_0 and γ_p were derived to be used primarily for the ρ_∞-Bathe method.

$$\gamma_0 = \frac{2 - \sqrt{2 + 2\rho_\infty}}{1 - \rho_\infty}; \qquad \gamma_0 = 0.5 \ \text{ if } \ \rho_\infty = 1 \tag{36}$$

$$\gamma_p = \frac{\rho_\infty + 2 - \sqrt{\rho_\infty^2 - 2\rho_\infty - 2}}{3(\rho_\infty + 1)}; \quad \rho_\infty \in \left(-1, 1 - \sqrt{3}\right] \tag{37}$$

where γ_0 achieves second-order accuracy while minimizing period elongation error, and γ_p achieves third-order accuracy. In Fig. 4, we illustrate the optimized splitting ratios γ_0 and γ_p in relation to ρ_∞, accompanied by the stable region defined in (23). The results show that both optimized splitting ratios are within the stable ranges. More specifically, the stable range of γ in the ρ_∞-Bathe method is divided into two distinct regions. Within these regions, γ_0 is the optimized splitting ratio for $0<\gamma<1$, whereas γ_p is the optimized splitting ratio for $2/(1-\rho_\infty) < \gamma$.

4. Stability analysis for the implicit β_1/β_2-Bathe scheme

In this section we focus on the implicit β_1/β_2-Bathe scheme, which we showed to be very effective in the solution of wave propagations.

4.1. The β_1/β_2-Bathe implicit time integration scheme

As in the ρ_∞-Bathe scheme, the β_1/β_2-Bathe scheme [24,25] uses two sub-steps of size $\gamma\Delta t$ and $(1-\gamma)\Delta t$. For the first sub-step the trapezoidal rule is used

$$\mathbf{M}\,{}^{t+\gamma\Delta t}\ddot{\mathbf{U}} + \mathbf{C}\,{}^{t+\gamma\Delta t}\dot{\mathbf{U}} + \mathbf{K}\,{}^{t+\gamma\Delta t}\mathbf{U} = {}^{t+\gamma\Delta t}\mathbf{R} \tag{38}$$

$${}^{t+\gamma\Delta t}\mathbf{U} = {}^{t}\mathbf{U} + \frac{\gamma\Delta t}{2}\left({}^{t}\dot{\mathbf{U}} + {}^{t+\gamma\Delta t}\dot{\mathbf{U}}\right) \tag{39}$$

$${}^{t+\gamma\Delta t}\dot{\mathbf{U}} = {}^{t}\dot{\mathbf{U}} + \frac{\gamma\Delta t}{2}\left({}^{t}\ddot{\mathbf{U}} + {}^{t+\gamma\Delta t}\ddot{\mathbf{U}}\right) \tag{40}$$

In the second sub-step, this method introduces the parameters β_1 and β_2 to specify numerical dissipations, as given here

$$\mathbf{M}\,{}^{t+\Delta t}\ddot{\mathbf{U}} + \mathbf{C}\,{}^{t+\Delta t}\dot{\mathbf{U}} + \mathbf{K}\,{}^{t+\Delta t}\mathbf{U} = {}^{t+\Delta t}\mathbf{R} \tag{41}$$

$${}^{t+\Delta t}\mathbf{U} = {}^{t}\mathbf{U} + (\gamma\Delta t)\left((1-\beta_1)\,{}^{t}\dot{\mathbf{U}} + \beta_1\,{}^{t+\gamma\Delta t}\dot{\mathbf{U}}\right) + ((1-\gamma)\Delta t)\left((1-\beta_2)\,{}^{t+\gamma\Delta t}\dot{\mathbf{U}} + \beta_2\,{}^{t+\Delta t}\dot{\mathbf{U}}\right) \tag{42}$$

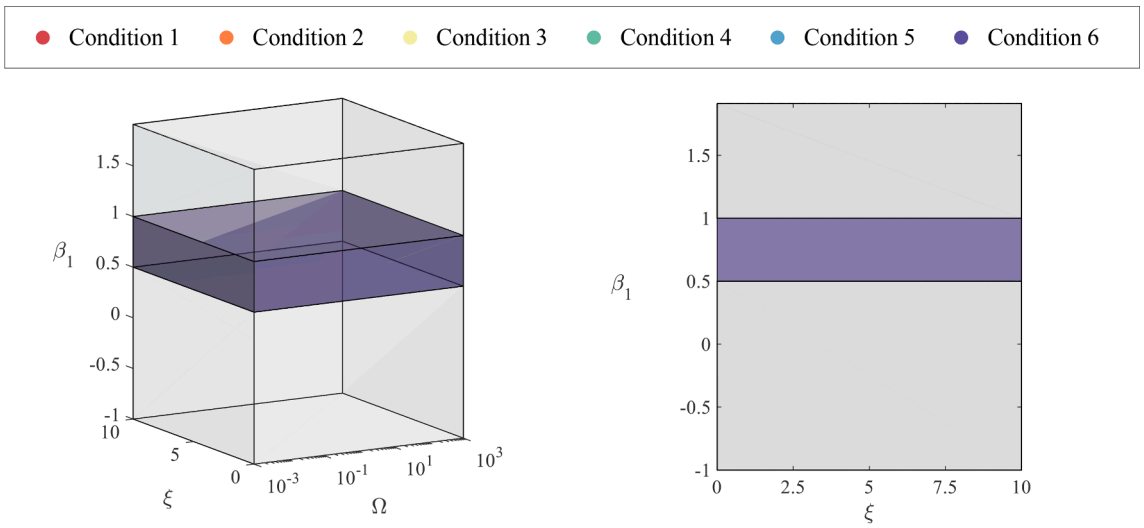

(a) Data points violating the conditions (b) Projection of Fig. 7(a) onto the ξ and β_1 plane

Fig. 7. Numerical test results of the β_1/β_2-Bathe method when $\gamma = (\beta_2 - 1)/(2\beta_1 - 2 + \beta_2)$ and $\beta_2 = [2(1-\beta_1) - 0.5(16\beta_1^2 - 24\beta_1 + 8)^{0.5}]$; Conditions (1–5) are associated with inequalities (8–12). Also, Condition 6 is violated when yielding a complex number. The gray-shaded regions, denoted by $\beta_1 < 1/2$ and $1 < \beta_1$, denote the region of stability from (55).

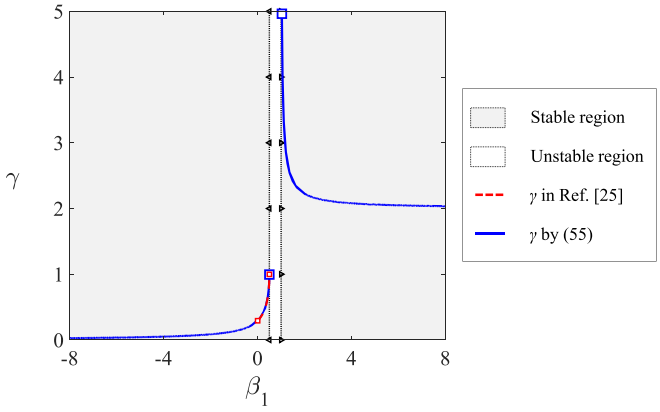

Fig. 8. The splitting ratio γ as a function of β_1 of the β_1/β_2-Bathe method with $\gamma = (\beta_2 - 1)/(2\beta_1 - 2 + \beta_2)$ and $\beta_2 = [2(1-\beta_1) - 0.5(16\beta_1^2 - 24\beta_1 + 8)^{0.5}]$; The previously reported ranges of β_1 in Ref. [25] are within the stable region given in (55).

$$ {}^{t+\Delta t}\dot{\mathbf{U}} = {}^{t}\dot{\mathbf{U}} + (\gamma\Delta t)\left((1-\beta_1)\,{}^{t}\ddot{\mathbf{U}} + \beta_1\,{}^{t+\gamma\Delta t}\ddot{\mathbf{U}}\right) + ((1-\gamma)\Delta t)\left((1-\beta_2)\,{}^{t+\gamma\Delta t}\ddot{\mathbf{U}} + \beta_2\,{}^{t+\Delta t}\ddot{\mathbf{U}}\right) \tag{43} $$

where β_1, β_2 and γ may vary for different numerical characteristics of the method [25]. In this study, we focus on the following two sets of the parameters recommended for $\rho_\infty = 0$ [25]:

$$ \text{Set 1:}\quad \gamma = \frac{\beta_2 - 1}{2\beta_1 - 2 + \beta_2},\ \beta_2 = \frac{1}{3 - 4\beta_1},\ \beta_1 \in \left(\frac{3}{4} - \frac{\sqrt{2}}{4}, \frac{1}{2}\right) \cup \left(\frac{1}{2}, \frac{3}{4}\right) \tag{44} $$

$$ \text{Set 2:}\quad \gamma = \frac{\beta_2 - 1}{2\beta_1 - 2 + \beta_2},\ \beta_1 \in (0, 0.5),\ \beta_2 = \left[2(1-\beta_1) - 0.5\left(16\beta_1^2 - 24\beta_1 + 8\right)^{0.5}\right] \tag{45} $$

where Set 1 are the parameters to achieve first-order accuracy and the same effective stiffness matrix for both sub-steps, and Set 2 are to achieve second-order accuracy. Note that the β_1/β_2-Bathe method with Set 2 is identical to the ρ_∞-Bathe method with ρ_∞=0, or the standard Bathe method (See Appendix A).

4.2. *Semi-analytical stability analysis of the β_1/β_2-Bathe method for Parameter Set 1*

We analyze the stability of the β_1/β_2-Bathe method with the Parameter Set 1, which uses the same effective stiffness matrix for both sub-steps. The stability analysis follows the procedure given in Section 3.2.

First, in case physical damping is present, only (8) can be analytically solved, as for the ρ_∞-Bathe method. Using the principal invariants of the β_1/β_2-Bathe method with Parameter Set 1, the values of Ω that satisfy $1 - A_1 + A_2 - A_3 = 0$ are

$$ \Omega_{(8),\xi\neq 0} = 0 \ \text{ or } \ (-\xi \pm \sqrt{\xi^2 - 1})(4\beta_1 - 5)^2 \tag{46} $$

which shows that all values of β_1 used in the Set 1 satisfy the inequality (8) for all ξ.

In the case of no damping, as in ρ_∞-Bathe method, inequalities (8–10) can be analytically solved, and the values of Ω for which the left-hand side of each inequality is zero are obtained as

$$ \Omega_{(8),\xi=0} = 0 \text{ or } \pm i\,(4\beta_1 - 5)^2 \tag{47} $$

$$ \Omega_{(9),\xi=0} = 0 \text{ or } \pm (4\beta_1 - 5)\frac{\sqrt{48\beta_1^2 - 24\beta_1 - 33}}{3} \tag{48} $$

$$ \Omega_{(10),\xi=0} = 0 \text{ or } \pm (4\beta_1 - 5)\sqrt{16\beta_1^2 - 24\beta_1 + 7} \tag{49} $$

Using Eqs. (46–49), the range of β_1 satisfying the inequalities (8–10)

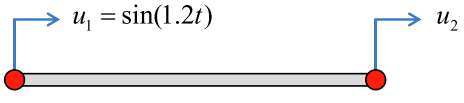

Fig. 9. A two-node truss element subjected to sinusoidal prescribed displacement; with initial values of $\dot{u}_1(0) = \ddot{u}_1(0) = u_2(0) = \dot{u}_2(0) = \ddot{u}_2(0) = 0$.

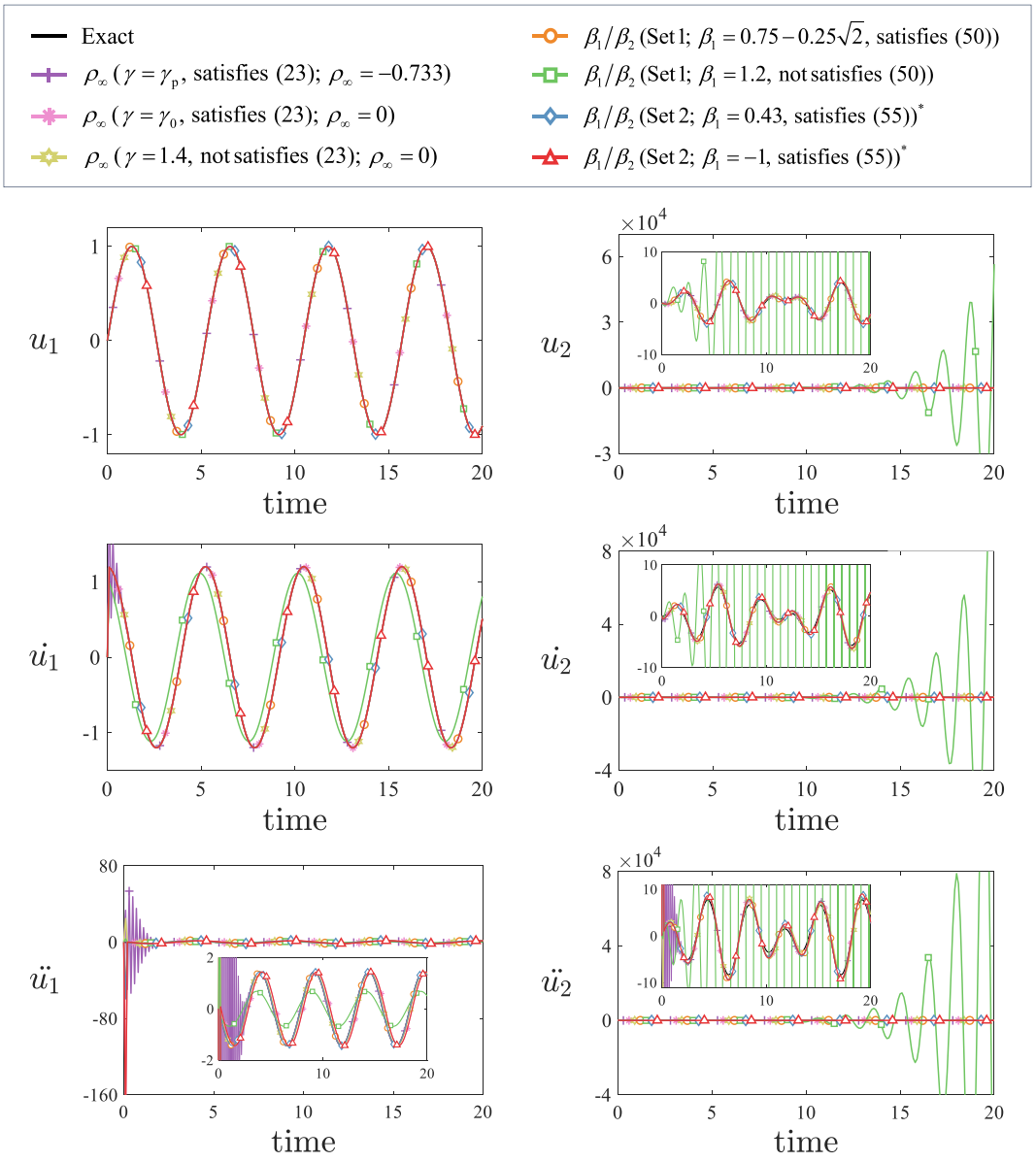

Fig. 10. Predictions of displacement, velocity, and acceleration for a 2-node truss example with $\mathbf{C} = \mathbf{0}$; Results of ρ_∞- Bathe (ρ_∞ in the figure) and β_1/β_2-Bathe (β_1/β_2 in the figure) methods. *β_1/β_2(Set 2; $\beta_1 = 0.43$) and β_1/β_2(Set 2; $\beta_1 = -1$) are identical to $\rho_\infty(\gamma = 0.650,\ \rho_\infty = 0)$ and $\rho_\infty(\gamma = 0.134,\ \rho_\infty = 0)$, respectively.

becomes

$$\beta_1 \in \left[\frac{3}{4} - \frac{\sqrt{2}}{4},\ \frac{3}{4} + \frac{\sqrt{2}}{4}\right] \tag{50}$$

Note that β_1=1/2 and 3/4 also need to be avoided to maintain the non-zero denominators in the constants of the method. Hence in this analysis using the analytically solvable inequalities we obtain a larger range of β_1, that is (50), than given in (44).

We next conduct a numerical stability analysis, applying all the inequalities derived from the Routh-Hurwitz criteria, as in ρ_∞-Bathe method. For the parameter β_1, we study the values [0.2, 1.3] using a 0.005 increment, while omitting values β_1=1/2 and 3/4 to prevent zero denominators. The region corresponding to (50) is shaded in gray.

As shown in Fig. 5, all inequalities from the Routh-Hurwitz criteria are satisfied within the range specified in (50).

Fig. 6 shows the splitting ratio γ as a function of β_1 in the range defined in (50) with the γ value for the β_1 range reported in Ref. [25], and it shows that the previously reported range of γ falls well within the range defined by (50).

4.3. Semi-analytical stability analysis of the β_1/β_2-Bathe method for Parameter Set 2

As in Sections 3.2 and 4.2, the stability characteristics of the β_1/β_2-Bathe method with Parameter Set 2 are first analyzed using inequality (8) in the presence of physical damping and inequalities (8–10) for zero damping. The values of Ω that render the left side of the considered inequalities zero are

$$\Omega_{(8),\xi\neq 0} = 0 \text{ or } \frac{4(\beta_1 - 1)\left(\xi \pm \sqrt{\xi^2 - 1}\right)}{\left(-2 + 2\beta_1 + \sqrt{4\beta_1^2 - 6\beta_1 + 2}\right)\left(-1 + 2\beta_1 + \sqrt{4\beta_1^2 - 6\beta_1 + 2}\right)} \tag{51}$$

$$\Omega_{(8),\xi=0} = 0 \text{ or } \frac{\pm 4i(\beta_1 - 1)}{\left(-2 + 2\beta_1 + \sqrt{4\beta_1^2 - 6\beta_1 + 2}\right)\left(-1 + 2\beta_1 + \sqrt{4\beta_1^2 - 6\beta_1 + 2}\right)} \tag{52}$$

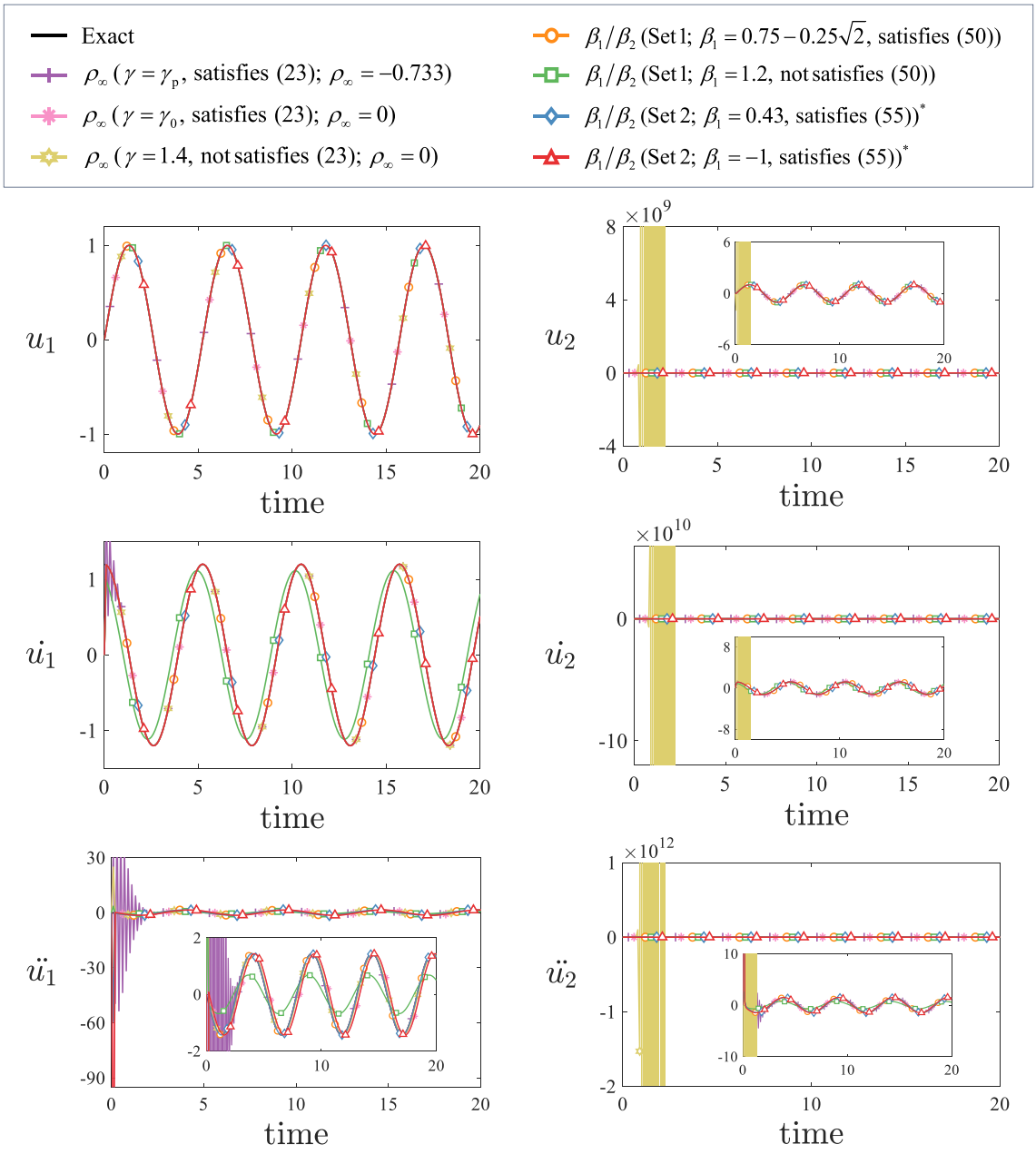

Fig. 11. Predictions of displacement, velocity, and acceleration for a 2-node truss example with $\mathbf{C} \neq \mathbf{0}$. Results of ρ_∞-Bathe and β_1/β_2-Bathe methods. *β_1/β_2(Set 2; $\beta_1 = 0.43$) and β_1/β_2(Set 2; $\beta_1 = -1$) are identical to $\rho_\infty(\gamma = 0.650,\ \rho_\infty = 0)$ and $\rho_\infty(\gamma = 0.134,\ \rho_\infty = 0)$, respectively.

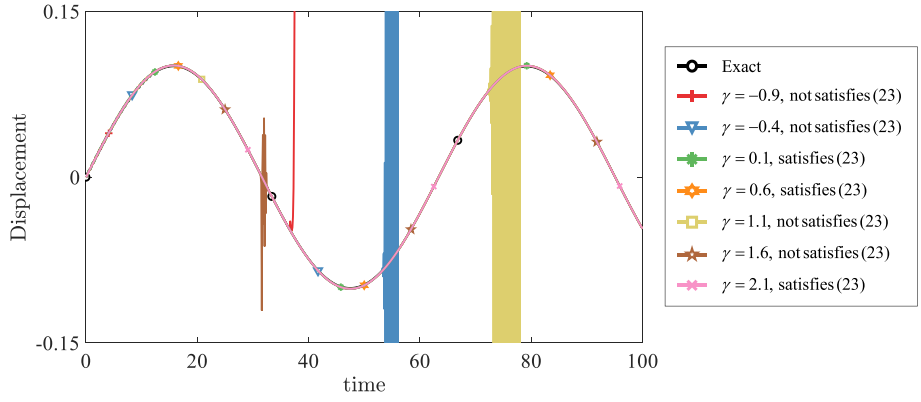

Fig. 12. Predicted displacements in the nonlinear spring example; the ρ_∞-Bathe method with ρ_∞=0 and various splitting ratios;

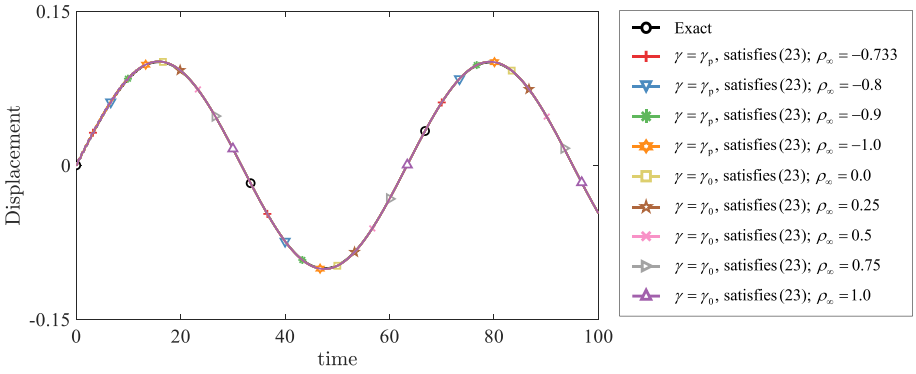

Fig. 13. Predicted displacements in the nonlinear spring example; the ρ_∞-Bathe method with various values of ρ_∞ and corresponding optimized splitting ratios;

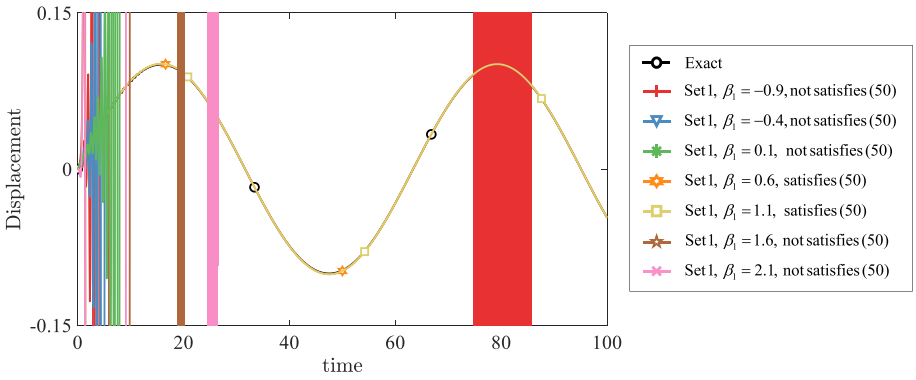

Fig. 14. Predicted displacements in the nonlinear spring example; the β_1/β_2-Bathe method with Parameter Set 1 and various values of β_1;

$$\Omega_{(9),\xi=0} = 0 \text{ or } \pm \frac{2\sqrt{-12\beta_1^2 + 18\beta_1 - 6}\,\sqrt{4\beta_1^2 - 6\beta_1 + 2}}{3\left(-1 + 2\beta_1 + \sqrt{4\beta_1^2 - 6\beta_1 + 2}\right)(2\beta_1 - 1)\left(-2 + 2\beta_1 + \sqrt{4\beta_1^2 - 6\beta_1 + 2}\right)} \tag{53}$$

$$\Omega_{(10),\xi=0} = 0 \tag{54}$$

Note that $\beta_1 = 1/2$ or 1 should also be avoided to maintain a non-zero denominator in the evaluation of γ and for $1/2 < \beta_1 < 1$, β_2 becomes a complex number. Therefore, as Eqs. (51–54) indicate all other values of β_1 provide stable solutions, and the applicable ranges of β_1 that satisfy all six conditions are

$$\beta_1 \in \left(-\infty, \frac{1}{2}\right) \cup (1, \infty) \tag{55}$$

We then perform the numerical stability analysis of the β_1/β_2-Bathe method with Parameter Set 2. The data set is the same as the one used in Section 4.2, except that we use the range $\beta_1 \in [-1, 2]$. As shown in Fig. 7, all conditions are fulfilled outside the range $0.5 \le \beta_1 \le 1$.

In Fig. 8, we show the splitting ratio γ versus β_1 in the range specified by (55) alongside the γ values for the β_1 range reported in Ref. [25]. We see that the previously reported γ range in Ref. [25] falls well within the range defined by (55). Note that the range of β_1 defined in (55) corresponds to $\gamma \in (0, 1) \cup (2, \infty)$ which is the range specified by (23) with $\rho_\infty = 0$ because the β_1/β_2-Bathe method with Parameter Set 2 is identical to the ρ_∞-Bathe method with ρ_∞=0.

5. Numerical examples

We present here two numerical examples to illustrate the findings given in the earlier sections. In the following examples, we consider various values of (γ, ρ_∞) and (β_1, β_2) for the ρ_∞-Bathe and β_1/β_2-Bathe methods. We use both parameter sets that satisfy the stability conditions, Eqs. (23), (50), or (55) (or fall within the previously reported ranges), as well as those that do not.

5.1. A linear finite element under sinusoidal prescribed displacement

We first consider the truss example with two degrees of freedom depicted in Fig. 9, subjected to the displacement $u = \sin(1.2t)$ at node 1. The objective in Ref. [37] was to evaluate the accuracy and stability of a time integration scheme under imposed displacements as part of a patch test. In this model problem we use

$$\mathbf{M} = \frac{1}{6}\begin{bmatrix} 2 & 1 \\ 1 & 2 \end{bmatrix}, \quad \mathbf{K} = \begin{bmatrix} 1 & -1 \\ -1 & 1 \end{bmatrix}, \quad \mathbf{C} = \begin{bmatrix} 5 & -5 \\ -5 & 5 \end{bmatrix} \tag{56}$$

where $\mathbf{M}, \mathbf{K}$ and $\mathbf{C}$ are the mass, stiffness, and damping matrices, respectively. Although exact expressions for the velocity and acceleration at node 1 are available, we employ the *exact imposed displacement* with the *numerically computed velocity and acceleration* at node 1 to adhere to what is done in practical engineering analyses [37]. We consider the solution with the damping specified in Eqs. (56) and without physical damping, that is, using $\mathbf{C} = \mathbf{0}$, and employ various parameter sets.

Figs. 10 and 11 show the results of the 2-node truss problem without and with damping, respectively. As expected, the ρ_∞-Bathe method with the values γ_p and $\rho_\infty = 1 - \sqrt{3}$ exhibits oscillations in the first few steps, eventually delivering accurate solutions. However, using the ρ_∞-Bathe method with γ=1.4 shows stability without damping but the solution diverges when the damping is included, consistent with the results given in Section 3.2. Using the β_1/β_2-Bathe scheme with Parameter Set 1 and β_1=1.2, the solution is stable when the damping is not included but diverges with the damping included, as predicted in Section 4.2. When

employing parameters that meet the stability conditions, both methods offer stable and accurate solutions, and thus successfully pass the imposed displacements patch test.

5.2. Nonlinear spring example

Next, we solve a nonlinear spring example with varying damping and stiffness. The differential equation solved is

$$\ddot{u}(t) + C(t)\dot{u}(t) + 100\tanh(u(t)) = 10\sin(0.1\,t) \tag{57}$$

where the initial displacement and velocity are $u(0) = 0$ and $\dot{u}(0) = 0$. The damping is given as

$$C(t) = (t-10)H(t-10), \quad t > 0 \tag{58}$$

where H is the unit step function. We perform the simulation from time 0 to 100 with $\Delta t = 0.1$. In this example, since the damping and stiffness vary with time t, we explore the stability of the time integration scheme when used with changing stiffness and damping values.

Fig. 12 shows the results of the nonlinear spring example using the ρ_∞-Bathe method with various γ and ρ_∞ values. For the ρ_∞-Bathe method, the applicable stable regions of γ are $0<\gamma<1$ and $2/(1-\rho_\infty) < \gamma$. The γ values that adhere to these ranges yield stable solutions, whereas using γ values outside leads to divergence in the solutions. Fig. 13 shows that when applying the ρ_∞-Bathe method with the optimized splitting ratios – so that all parameter sets satisfy the stability condition – the results are consistently stable.

Figs. 14 and 15 present the results when using the β_1/β_2-Bathe scheme with Parameter Set 1 and Parameter Set 2, respectively. As shown in Figs. 14 and 15, the solutions remain stable when the value of β_1 corresponds to the regions of stability identified in Sections 4.2 and 4.3, while values of β_1 outside the defined ranges in (50) and (55) lead to divergence of the numerical solution.

6. Concluding remarks

We focused on the stability of the ρ_∞-Bathe and β_1/β_2-Bathe time integration methods when physical damping is present and used a semi-analytical stability analysis. Specifically, we first determined stability regions by evaluating solvable inequalities of the Routh-Hurwitz conditions for both, the damped and undamped situations. Subsequently, we performed numerical tests to see whether for these regions in fact all stability conditions of Routh-Hurwitz stability conditions are satisfied.

Using the semi-analytical approach, we identified the parameters ranges that yield stable solutions for the ρ_∞-Bathe and β_1/β_2-Bathe methods in the presence of physical damping and found that all previously reported useful Parameter Sets for stability are within these ranges. This includes the optimized γ values for the ρ_∞-Bathe method proposed in Refs [26–29], and the recommended parameter sets for the β_1/β_2-Bathe method [25]. Also, the methods employing parameters within these ranges successfully passed the displacement imposition patch test. In addition, the results of the stability analyses were validated using a simple nonlinear spring example in which the stiffness and damping changed during the time integration.

While stability analyses of time integration methods have been primarily conducted in the absence of physical damping assuming that physical damping will increase the stability of a time integration scheme, our analysis indicates that physical damping may induce an unstable time integration. Fig. 16 shows the spectral radii ρ(A) of the ρ_∞-Bathe and β_1/β_2-Bathe methods with parameter sets not satisfying the stability conditions. Notably, while damping augments stability in the β_1/β_2-Bathe method with Parameter Set 1, it destabilizes the

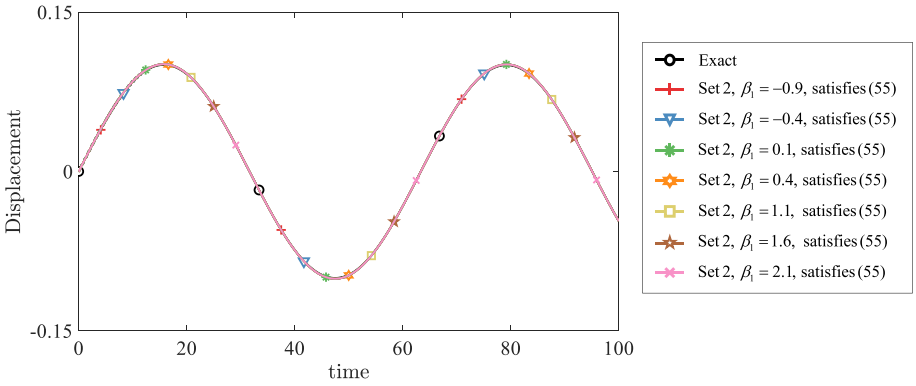

Fig. 15. Predicted displacements in the nonlinear spring example using the β_1/β_2-Bathe method with Parameter Set 2 and various values of β_1; the same results are obtained using the ρ_∞-Bathe method with ρ_∞=0 and $\gamma = (2\sqrt{4\beta_1^2 - 6\beta_1 + 2} + 4\beta_1 - 3)/(2\beta_1 + \sqrt{4\beta_1^2 - 6\beta_1 + 2} - 2)$;

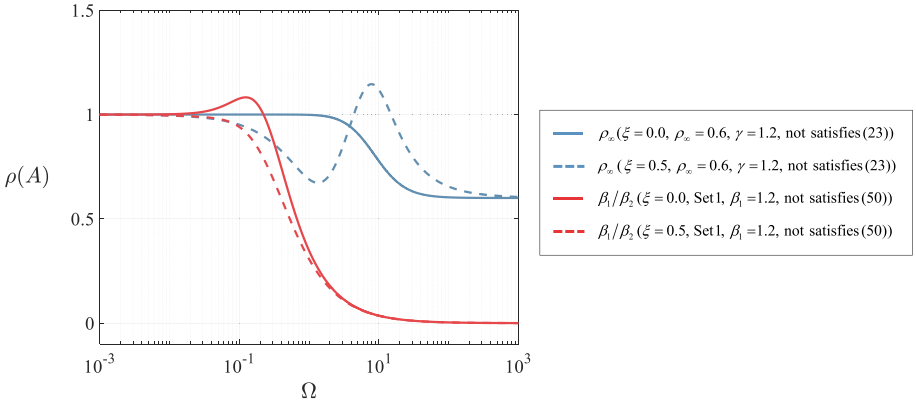

Fig. 16. Spectral radii of the ρ_∞-Bathe (with ρ_∞=0.6 and γ=1.2) and β_1/β_2-Bathe (with β_1=1.2) methods for various values of ξ.

ρ_∞-Bathe method. This underscores that physical damping may not be beneficial for the stability of a time integration method, highlighting the need for comprehensive stability analyses that incorporate the effects of physical damping.

In this paper we performed semi-analytical stability analyses, because we found the expressions we used were too complex to solve only analytically. Further research is needed to identify more tractable stability conditions that can be solved fully analytically. The results we presented in this paper may be a foundation towards that aim.

CRediT authorship contribution statement

Chanju Lee: Formal analysis, Investigation, Writing – original draft. **Klaus-Jürgen Bathe:** Conceptualization, Investigation, Writing – review & editing. **Gunwoo Noh:** Conceptualization, Investigation, Writing – review & editing.

Declaration of competing interest

The authors declare that they have no known competing financial interests or personal relationships that could have appeared to influence the work reported in this paper.

Data availability

Data will be made available on request.

Acknowledgments

This work was partly supported by the National Research Foundation of Korea (NRF) funded by the Ministry of Science and ICT (Grant No. NRF-2021R1C1C1011494 and RS-2023-00220762).

Appendix A. The ρ_∞-Bathe method with ρ_∞=0 and the β_1/β_2-Bathe method with Set 2 are identical

It is clear that the relations in the first sub-step of the ρ_∞-Bathe method and the β_1/β_2-Bathe method are identical as

$$ {}^{t+\gamma\Delta t}\mathbf{U} = {}^{t}\mathbf{U} + \frac{\gamma\Delta t}{2}\left({}^{t}\dot{\mathbf{U}} + {}^{t+\gamma\Delta t}\dot{\mathbf{U}}\right) \tag{A1} $$

$$ {}^{t+\gamma\Delta t}\dot{\mathbf{U}} = {}^{t}\dot{\mathbf{U}} + \frac{\gamma\Delta t}{2}\left({}^{t}\ddot{\mathbf{U}} + {}^{t+\gamma\Delta t}\ddot{\mathbf{U}}\right) \tag{A2} $$

Therefore, only the second sub-step is compared. In the second sub-step, considering the ρ_∞-Bathe method with Eqs. (19–20) and $\gamma = (2\sqrt{4\beta_1^2 - 6\beta_1 + 2} + 4\beta_1 - 3)/(2\beta_1 + \sqrt{4\beta_1^2 - 6\beta_1 + 2} - 2)$, Eqs. (17) and (18) become

$$ {}^{t+\Delta t}\mathbf{U} = {}^{t}\mathbf{U} + {}^{t}\dot{\mathbf{U}}\alpha_1 + {}^{t+\gamma\Delta t}\dot{\mathbf{U}}\alpha_2 + {}^{t}\ddot{\mathbf{U}}\alpha_3 + {}^{t+\gamma\Delta t}\ddot{\mathbf{U}}\alpha_3 + {}^{t+\Delta t}\ddot{\mathbf{U}}\alpha_4 \tag{A3} $$

$$ {}^{t+\Delta t}\dot{\mathbf{U}} = {}^{t}\dot{\mathbf{U}} + {}^{t}\ddot{\mathbf{U}}\alpha_2 + {}^{t+\gamma\Delta t}\ddot{\mathbf{U}}\alpha_2 + {}^{t+\Delta t}\ddot{\mathbf{U}}\alpha_5 \tag{A4} $$

where,

$$ \alpha_1 = \frac{\Delta t\left(\sqrt{4\beta_1^2 - 6\beta_1 + 2} + 2\beta_1\right)}{2}, $$

$$ \alpha_2 = -\frac{\Delta t\left(2\beta_1 + \sqrt{4\beta_1^2 - 6\beta_1 + 2} - 2\right)}{2}, $$

$$ \alpha_3 = -\frac{\Delta t^2\left(4\beta_1\sqrt{4\beta_1^2 - 6\beta_1 + 2} + 8\beta_1^2 - 3\sqrt{4\beta_1^2 - 6\beta_1 + 2} - 12\beta_1 + 4\right)}{2}, $$

$$ \alpha_4 = \Delta t^2(-2\beta_1 + 1)\left(2\sqrt{4\beta_1^2 - 6\beta_1 + 2} + 4\beta_1 - 3\right), $$

$$ \alpha_5 = \Delta t\left(\sqrt{4\beta_1^2 - 6\beta_1 + 2} + 2\beta_1 - 1\right) $$

In the β_1/β_2-Bathe method with Set 2, the relations in the second sub-step, Eqs. (42) and (43), become

$$ {}^{t+\Delta t}\mathbf{U} = {}^{t}\mathbf{U} + {}^{t}\dot{\mathbf{U}}\alpha_1 + {}^{t+\gamma\Delta t}\dot{\mathbf{U}}\alpha_2 + {}^{t}\ddot{\mathbf{U}}\alpha_3 + {}^{t+\gamma\Delta t}\ddot{\mathbf{U}}\alpha_3 + {}^{t+\Delta t}\ddot{\mathbf{U}}\alpha_4 \tag{A5} $$

$$ {}^{t+\Delta t}\dot{\mathbf{U}} = {}^{t}\dot{\mathbf{U}} + {}^{t}\ddot{\mathbf{U}}\alpha_2 + {}^{t+\gamma\Delta t}\ddot{\mathbf{U}}\alpha_2 + {}^{t+\Delta t}\ddot{\mathbf{U}}\alpha_5 \tag{A6} $$

which are the relations in the second sub-step of the ρ_∞-Bathe method, Eqs. (A3) and (A4).

References

[1] Bathe KJ. The finite element method. In: Linderberg T, Wah B, editors. Encyclopedia of computer science and engineering. Hoboken, New Jersey: J. Wiley and Sons; 2009. p. 1253–64.

[2] Bathe KJ. Frontiers in finite element procedures & applications. In: Topping BHV, Iványi P, editors. Chapter 1 in Computational methods for engineering technology. Stirlingshire, Scotland: Saxe-Coburg Publications; 2014.

[3] Bathe KJ. Finite element procedures. 2nd ed. Bathe KJ, Watertown: MA; also published by Higher Education Press China; 2016.

[4] Newmark NM. A method of computation for structural dynamics. J Eng Mech Divs 1959;85(3):67–94.

[5] Wilson EL, Farhoomand I, Bathe KJ. Nonlinear dynamic analysis of complex structures. Int J Earthq Eng Struct Dyn 1973;1:241–52.

[6] Hilber HM, Hughes TJR, Taylor RL. Improved numerical dissipation for time integration algorithms in structural dynamics. Earthq Eng Struct Dyn 1977;5(3):283–92.

[7] Wood WL, Bossak M, Zienkiewicz OC. An alpha modification of Newmark's method. Int J Numer Methods Eng 1980;15(10):1562–6.

[8] Shao HP, Cai CW. A three parameters algorithm for numerical integration of structural dynamic equations. Chin J Appl Mech 1988;5(4):76–81.

[9] Chung J, Hulbert GM. A time integration algorithm for structural dynamics with improved numerical dissipation: the generalized-α method. J Appl Mech (ASME) 1993;60(2):371–5.

[10] Tamma KK, Zhou X, Sha D. The time dimension: A theory towards the evolution, classification, characterization and design of computational algorithms for transient/dynamic applications. Arch Comput Methods Eng 2000;7(2):67–290.

[11] Soares D. An improved adaptive formulation for explicit analyses of wave propagation models considering locally-defined self-adjustable time-integration parameters. Comput Methods Appl Mech Eng 2022;399:115324.

[12] Soares D. An enhanced explicit–implicit time-marching formulation based on fully-adaptive time-integration parameters. Comput Methods Appl Mech Eng 2023;403:115711.

[13] Song C, Eisenträger S, Zhang X. High-order implicit time integration scheme based on Padé expansions. Comput Methods Appl Mech Eng 2022;390:114436.

[14] Bathe KJ, Baig MMI. On a composite implicit time integration procedure for nonlinear dynamics. Comput Struct 2005;83(31–32):2513–4.

[15] Bathe KJ. Conserving energy and momentum in nonlinear dynamics: a simple implicit time integration scheme. Comput Struct 2007;85(7–8):437–45.

[16] Wen WB, Wei K, Lei HS, Duan SY, Fang DN. A novel sub-step composite implicit time integration scheme for structural dynamics. Comput Struct 2017;182:176–86.

[17] Zhang HM, Xing YF. Optimization of a class of composite method for structural dynamics. Comput Struct 2018;202:60–73.

[18] Li J, Yu K, Li X. A novel family of controllably dissipative composite integration algorithms for structural dynamic analysis. Nonlinear Dyn 2019;96(4):2475–507.

[19] Li J, Yu K. A novel family of composite sub-step algorithms with desired numerical dissipations for structural dynamics. Arch Appl Mech 2020;90(4):737–72.

[20] Zhang J. A-stable two-step time integration methods with controllable numericaldissipation for structural dynamics. Int J Numer Methods Eng 2020;121:54–92.

[21] Ji Y, Xing YF. An optimized three-sub-step composite time integration method with controllable numerical dissipation. Comput Struct 2020;231:106210.

[22] Zhang H, Zhang R, Xing Y, Masarati P. On the optimization of n-sub-step composite time integration methods. Nonlinear Dyn 2020;102(3):1939–62.

[23] Wen W, Deng S, Wang N, Duan S, Fang D. An improved sub-step time-marching procedure for linear and nonlinear dynamics with high-order accuracy and high-efficient energy conservation. Appl Math Model 2021;90:78–100.

[24] Malakiyeh MM, Shojaee S, Bathe KJ. The Bathe time integration method revisited for prescribing desired numerical dissipation. Comput Struct 2019;212:289–98.

[25] Malakiyeh MM, Shojaee S, Hamzehei-Javaran S, Bathe KJ. New insights into the β_1/β_2-Bathe time integration scheme when L-stable. Comput Struct 2021;245:106433.

[26] Noh G, Bathe KJ. The Bathe time integration method with controllable spectral radius: the ρ_∞-Bathe method. Comput Struct 2019;212:299–310.

[27] Noh G, Bathe KJ. For direct time integrations: A comparison of the Newmark and ρ_∞-Bathe schemes. Comput Struct 2019;225:106079.

[28] Kwon S-B, Bathe KJ, Noh G. Selecting the load at the intermediate time point of the ρ_∞-Bathe time integration scheme. Comput Struct 2021;254:106559.

[29] Choi B, Bathe KJ, Noh G. Time Splitting ratio in the ρ∞-Bathe method time integration method for higher-order accuracy in structural dynamics and heat transfer. Comput Struct 2022;270:106814.

[30] Bathe KJ, Noh G. Insight into an implicit time integration scheme for structural dynamics. Comput Struct 2012;98:1–6.

[31] Noh G, Bathe KJ. Further insights into an implicit time integration scheme for structural dynamics. Comput Struct 2018;202:15–24.

[32] Kim W, Choi SY. An improved implicit time integration algorithm: the generalized composite time integration algorithm. Comput Struct 2018;196:341–54.

[33] Li J, Zhao R, Yu K, Li X. Directly self-starting higher-order implicit integration algorithms with flexible dissipation control for structural dynamics. Comput Methods Appl Mech Eng 2022;389:114274.

[34] Li J, Li H, Yu K, Zhao R. 2022a. High-order accurate multi-sub-step implicit integration algorithms with dissipation control for second-order hyperbolic problems. arXiv:2209.13820 URL: https://doi.org/10.48550/arXiv.2209.13.

[35] Noh G, Ham S, Bathe KJ. Performance of an implicit time integration scheme in the analysis of wave propagations. Comput Struct 2013;123:93–105.

[36] Kwon S-B, Bathe KJ, Noh G. An analysis of implicit time integration schemes for wave propagations. Comput Struct 2020;230:106188.

[37] Noh G, Bathe KJ. Imposing displacements in implicit direct time integration & a patch test. Adv Eng Softw 2023;175:103286.

[38] Noh G, Bathe KJ. An explicit time integration scheme for the analysis of wave propagations. Comput Struct 2013;129:178–93.

[39] Li J, Li H, Lian Y, Zhao R, Yu K. A suite of second-order composite sub-step explicit algorithms with controllable numerical dissipation and maximal stability bounds. Appl Math Model 2023;114:601–26.

[40] Li J, Yu K, Zhao R. Two third-order explicit integration algorithms with controllable numerical dissipation for second-order nonlinear dynamics. Comput Methods Appl Mech Eng 2022;395:114945.

[41] Malakiyeh MM, Shojaee S, Hamzehei-Javaran S, Bathe KJ. The explicit β_1/β_2-Bathe time integration method. Comput Struct 2023;286:107092.

[42] Lambert JD. Computational methods in ordinary differential equations. 2nd ed. John Wiley & Sons; 1974.